Phase diagram and stability of skyrmion configurations in anti-ferromagnetic materials lacking inversion symmetry

A.E. Baerends
Bachelor Thesis
Under the supervision of
dr. R.A. Duine
Institute of Theoretical Physics, Utrecht University

June 16, 2015

Abstract

We investigate the skyrmion configuration in anti-ferromagnetic materials lacking inversion symmetry, specifically its stability compared to other phases in such materials. A model for magnetic structures in anti-ferromagnetic materials is used to calculate the energies of skyrmion states, and homogeneous and spiral states. One finds that the skyrmion configuration can exist as a stable state among homogeneous and spiral states. At the same time, a point-by-point approach lets us construct a primitive phase diagram, which can be used to guide future Monte-Carlo simulations.

Contents

1 Introduction

When investigating magnetic materials and their properties, one often investigates the exchange energy between the magnetic spins, for it determines the total energy of the system dominantly. Magnetic materials can be divided into two categories depending on the sign of exchange coupling: *ferromagnetic* if the magnetic spins are aligned parallel, and *anti-ferromagnetic* if the spins are aligned anti-parallel[1]. A schematic representation of the differences in spin alignment between these two types of materials is shown in Fig. 1. Alignments can also be caused by external magnetic fields; at sufficient strength, the external field forces the spins inside the magnetic material to align themselves along this external field.

(a) A ferromagnetic material.

(b) An anti-ferromagnetic material.

Figure 1: Schematic representations of magnetic spins at spontaneous magnetization in ferromagnetic and anti-ferromagnetic materials.

In a limited selection of materials, other energy terms may arise, one of which is the *Dzyaloshinskii-Moriya interaction*, forcing the system to form different kinds of spiral structures[2,3]. The Dzyaloshinskii-Moriya interaction causes neighbouring spins to slightly deviate from a perfect alignment, leading to a preference in magnetization at zero external field. One kind of spiral structures resulting form the Dzyaloshinskii-Moriya interaction is the *skyrmion*, a rotationally invariant topological object formed out of a spiraling magnetization[4]. Two main types of skyrmions exist: the *hedgehog* configuration of Fig. 2a, and the *vortex* configuration of Fig. 2b. Skyrmions are already experimentally observed in a multitude of materials, mainly ferromagnetic ones[5,6], and are expected to have a noticeable commercial potential for application. This is because skyrmions can be manipulated easily with low electrical current density[7]. Their small size — of the order of nanometers — and low electricity consumption are attractive for future memory storage and computation devices.

In this Thesis, we construct phase diagrams of anti-ferromagnetic materials, and attempt to find instances — if any — where skyrmion configurations can be the lowest energy states for these materials, and under which circumstances. Firstly, we look at skyrmions in ferromagnetic materials in

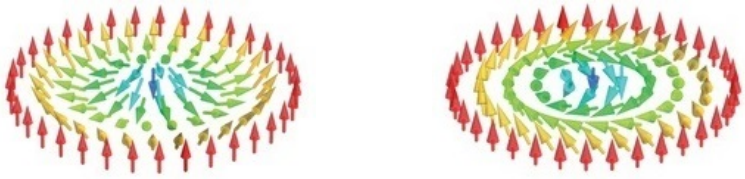

(a) Hedgehog configuration. (b) Vortex configuration.

Figure 2: The two most common skyrmion configurations. Figures reprinted from Fert *et al.*[7].

order to gain a better understanding of skyrmion configurations in general. Secondly, we construct a model for finding modulated structures in anti-ferromagnetic materials, resulting from Dzyaloshinskii-Moriya interactions. Through simplifications and justified assumptions, a model for various possible modulated states inside an anti-ferromagnetic material is constructed, which forms the basis of involved phase diagrams. Thirdly, we calculate the energy of a skyrmion configuration inside such anti-ferromagnetic materials. We then apply this energy to find out whether or not skyrmion configurations are the lowest energy states under specific circumstances, and where these configurations are located in aforementioned phase diagrams.

1.1 Skyrmions in ferromagnetic materials at zero temperature

To understand the basic properties of skyrmions, we begin our investigation at the simplest case: a single skyrmion in ferromagnetic material at zero temperature. In general, the energy of a magnetic material is given by[8]:

$$W[\mathbf{m}(\mathbf{x})] = \int \mathrm{d}\mathbf{x} \left\{ -\frac{J_s}{2}\mathbf{m}\cdot\nabla^2\mathbf{m} + \frac{C}{2}\mathbf{m}\cdot(\nabla\times\mathbf{m}) + K(1-m_z^2) + \mu_0 hM(1-m_z) - \mu_0 M\mathbf{m}\cdot\mathbf{h}_\mathrm{d} \right\}. \quad (1)$$

In the above equation, the present parameters are J_s as the spin stiffness, C as the Dzyaloshinskii-Moriya interaction constant, K as the anisotropy constant, and μ_0 as the vacuum permeability. Furthermore, we assume the external magnetic field H to be positively valued, and to be applied in the $\hat{z}$-direction, while $\mathbf{h}_\mathrm{d}$ is the demagnetizing field. Finally, M is the saturation magnetization and $\mathbf{m}(\mathbf{x})$ its associated unit vector, such that $\mathbf{M}(\mathbf{x}) = M\mathbf{m}(\mathbf{x})$ is the magnetization vector of the skyrmion.

Since skyrmions tend to be cylindrical in nature[4], we can write $\mathbf{m}(\mathbf{x})$ in cylindrical coordinates $\mathbf{x} = (\rho, \phi, z)$ as

$$\mathbf{m}(\mathbf{x}) = \sin\theta\cos\phi_0\hat{\rho} + \sin\theta\sin\phi_0\hat{\phi} + \cos\theta\hat{z}, \quad (2)$$

where θ can depend on cylindrical coordinates $\mathbf{x} = (\rho, \phi, z)$, and the angle ϕ_0 is a constant which determines the form of the skyrmion; hedgehog-like ($\phi_0 = 0$), or vortex-like ($\phi_0 = \frac{\pi}{2}$). An important property of skyrmions is the magnetization at the centre of a skyrmion, which is opposite to the direction of the external magnetic field. We now assume rotational symmetry in the $\hat{\phi}$-direction and translational symmetry in the $\hat{z}$-direction, resulting in θ solely depending on ρ.

For simplicity, we further restrict our investigation to two-dimensional materials. In the two-dimensional case, for example a thin layer of cobalt between two layers of platinum [9], Equation (1) reduces to:

$$\tilde{W}[\mathbf{m}(\mathbf{x})] = t_c \int \mathrm{d}\mathbf{x} \left\{ -\frac{J_s}{2}\mathbf{m} \cdot \nabla^2 \mathbf{m} + \frac{C}{2}\left(\hat{y} \cdot \left(\mathbf{m} \times \frac{\partial \mathbf{m}}{\partial x} \right) \right.\right.$$
$$\left.\left. -\hat{x} \cdot \left(\mathbf{m} \times \frac{\partial \mathbf{m}}{\partial y} \right) \right) + K(1 - m_z^2) + \mu_0 h M (1 - m_z) - \mu_0 M \mathbf{m} \cdot \mathbf{h_d} \right\}, \quad (3)$$

where t_c is the thickness of the film in the $\hat{z}$-direction.

Furthermore, let us assume the system is completely isotropic and lacks a demagnetizing field, giving us $K = 0$ and $\mathbf{h}_\mathrm{d} = 0$. Then, using the parametrization for $\mathbf{m}$ given in Equation (2), this yields:

$$w[\theta(\rho)] \equiv \frac{\tilde{W}[\theta(\rho)]}{2\pi t_c} = \int \mathrm{d}\rho \left\{ \frac{J_s}{2}\left(\left(\frac{\mathrm{d}\theta}{\mathrm{d}\rho} \right)^2 + \frac{\sin^2\theta}{\rho^2} \right) \right.$$
$$\left. + \frac{C}{2}\cos\phi_0 \left(\frac{\mathrm{d}\theta}{\mathrm{d}\rho} + \frac{\sin\theta\cos\theta}{\rho} \right) + \mu_0 h M (1 - \cos\theta) \right\} \rho. \quad (4)$$

Using the Euler-Lagrange equations and substituting ρ with the dimensionless variable $\tilde{\rho} = \frac{J_s}{C}\rho$ yields

$$\frac{\mathrm{d}^2\theta}{\mathrm{d}\tilde{\rho}^2} + \frac{1}{\tilde{\rho}}\frac{\mathrm{d}\theta}{\mathrm{d}\tilde{\rho}} + \cos\phi_0 \frac{\sin^2\theta}{\tilde{\rho}} - \frac{\sin\theta\cos\theta}{\tilde{\rho}^2} - \frac{h_r}{2}\cos\theta = 0, \quad (5)$$

where $h_r = 2\mu_0 h M J_s C^{-2}$. Typical values found for h_r suggest the skyrmion will be in the hedgehog configuration, yielding $\phi_0 = 0$. [8,9]. The presence of the goniometric terms $\cos\theta$ and $\sin\theta$ does not permit us to solve Eq. (5) analytically, and thus we solve this equation numerically.

For boundary conditions, we choose the external magnetic field to be in the positive $\hat{z}$-direction. This leads to $\theta(0) = \pi$ to resemble a negative $\hat{z}$-direction for the magnetization at the centre of the skyrmion $\tilde{\rho} = 0$, and $\theta(\tilde{\rho} \to \infty) = 0$ to resemble a positive $\hat{z}$-direction at $\tilde{\rho} = \infty$. The solution for $\theta(\tilde{\rho})$ using these boundary conditions is given in Figure 3.

One can note from Figure 3 that a higher value of the external magnetic field, h, results in a smaller skyrmion. This originates from the larger amount of energy spent on maintaining the centre magnetization opposite to the external magnetic field.

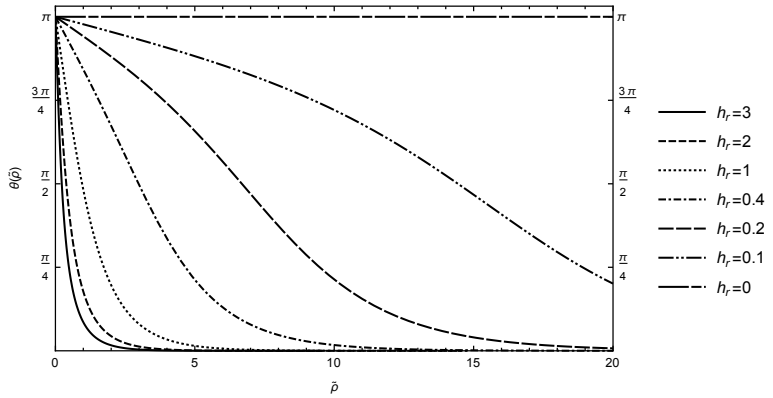

Figure 3: Numerical calculations of $\theta(\tilde{\rho})$ for different values of a single two-dimensional skyrmion at zero temperature.

2 Model for magnetic structures in anti-ferromagnetic materials

Now that the properties of skyrmions in ferromagnetic materials are known, we can look at anti-ferromagnetic materials for comparison. For this, we follow the discussion given by Bogdanov *et al.* (2002) [10] to determine the properties of structures inside anti-ferromagnetic materials. Among these structures, skyrmions *could* exist, a question that shall be answered in the next section.

2.1 Phenomenological model and simplification

Anti-ferromagnetic materials possess two sublattices of magnetization $\mathbf{M}_i$ for $i = 1{,}2$, whose vectors do not change their modulus $|\mathbf{M}_i| = M_s$ at temperatures sufficiently below the ordering temperature. Furthermore, these magnetization vectors can also be described by unity vectors $\mathbf{m}_i = \mathbf{M}_i/M_s$. For tetragonal anti-ferromagnetic crystals, the magnetic energy is given by:

$$\begin{aligned} W = \int \mathrm{d}V \Bigg\{ & \frac{\alpha}{2} \sum_{i=1}^{3} \left(\left(\frac{\partial \mathbf{m}_1}{\partial x_i} \right)^2 + \left(\frac{\partial \mathbf{m}_2}{\partial x_i} \right)^2 \right) + \alpha' \sum_{i=1}^{3} \left(\frac{\partial \mathbf{m}_1}{\partial x_i} \frac{\partial \mathbf{m}_2}{\partial x_i} \right) \\ & + \frac{\lambda}{2} \mathbf{m}_1 \cdot \mathbf{m}_2 - \mathbf{h} \cdot (\mathbf{m}_1 + \mathbf{m}_2) - \frac{\beta}{2} (m_{1z}^2 + m_{2z}^2) - \beta' m_{1z} m_{2z} \\ & - \mathbf{d} \cdot (\mathbf{m}_1 \times \mathbf{m}_2) + w_D \Bigg\} \end{aligned} \tag{6}$$

including inhomogenous ($\alpha,\ \alpha'$) and homogeneous (λ) parts of the coupling, and the interaction energy with the external field $\mathbf{h}$. Finally, w_D describes the Lifshitz invariant — which depends on the material used — for the

Dzyaloshinskii-Moriya coupling. In most cases, we assume the tetragonal axis of the anti-ferromagnetic crystal to be aligned along the z axis, *i.e.*, rotationally invariant structures in the material are then aligned along the z axis, and the basal plane of the material is then aligned along the xy plane. The behaviour of the material depends on whether the parameters d and w_D are zero or not. When both parameters are non-zero, the material can permit the formation of specific modulated states in which the magnetizations are oscillating.

Terms including the sublattice magnetization $\mathbf{m}_i$ can be rewritten using linear combinations of said sublattice magnetization. Let us define $\mathbf{m} = (\mathbf{m}_1 + \mathbf{m}_2)/2$ as the vector of total magnetization, and $\mathbf{l} = (\mathbf{m}_1 - \mathbf{m}_2)/2$ as the vector of staggered magnetization. Since $|\mathbf{m}_i| = 1$, the constraints $\mathbf{m} \cdot \mathbf{l} = 0$ and $\mathbf{m}^2 + \mathbf{l}^2 = 1$ are satisfied.

Often, the exchange coupling is the strongest among possible internal interactions, in particular homogeneous couplings, meaning exchanges of order λ are much more important than those of order d, β and β'. This permits us to simplify Eq. (6) by excluding gradients of $\mathbf{m}$:

$$\tilde{W} = \int \mathrm{d}V \left\{ A \sum_{i=1}^{3} \left(\frac{\partial \mathbf{l}}{\partial x_i} \right)^2 + \lambda \mathbf{m}^2 - 2\mathbf{m} \cdot \mathbf{h} + 2\mathbf{d} \cdot (\mathbf{m} \times \mathbf{l}) - B l_z^2 + w_D \right\}, \tag{7}$$

where $A = \alpha - \alpha'$ and $B = \beta - \beta'$.

Now define $\mathbf{n} = \mathbf{l}/|\mathbf{l}|$ as the unity vector parallel to the staggered magnetization vector. By assuming weak total magnetization, *i.e.* $|\vec{m}| \ll 1$, this implies $|\mathbf{l}| \simeq 1$, and thus minimizing energy $\tilde{W}$ of (7) independently with respect to $\mathbf{m}$ yields the following:

$$\mathbf{m} = -\frac{1}{\lambda} \left(\mathbf{n} \times (\mathbf{d} + \mathbf{n} \times \mathbf{h}) \right), \tag{8}$$

where $\mathbf{d} = (0,0,d)$.

Substituting Eq. (8) into Eq. (7) then results in the energy approximately as a function of $\mathbf{n}$:

$$\tilde{W} = \int \mathrm{d}V \left\{ A \sum_{i,j}^{3} \left(\frac{\partial n_i}{\partial x_j} \right)^2 - \frac{1}{\lambda} ((h_x + d n_y)^2 + (h_y - d n_x)^2 - (\mathbf{h} \cdot \mathbf{n})^2) - B n_z^2 + w_D(\mathbf{n}) \right\}. \tag{9}$$

For convenience, we shall write $\mathbf{n}(x, y)$ and $\mathbf{h}$ in spherical coordinates:

$$\mathbf{n} = (\sin\theta\cos\psi, \sin\theta\sin\psi, \cos\theta); \;\; \mathbf{h} = (h\sin\zeta\cos\eta, h\sin\zeta\sin\eta, h\cos\zeta).$$

The above choices for $\mathbf{n}$ and $\mathbf{h}$, and integrating (9) with respect to z, in a system with linear size L_z, $x_1 = x,\ x_2 = y$, yields:

$$\tilde{W} = L_z \int \mathrm{d}x\ \mathrm{d}y\ \left\{ A \sum_{i=1}^{2} \left(\left(\frac{\partial \theta}{\partial x_i} \right)^2 + \sin^2\theta \left(\frac{\partial \psi}{\partial x_i} \right)^2 \right) + w_D + \tilde{w} \right\}, \quad (10)$$

where $\tilde{w}$ is independent of spatial derivatives:

$$\begin{aligned} \lambda\tilde{w} &- (\lambda B - d^2 - h^2\cos^2\zeta)\cos^2\theta - (h^2\sin^2\zeta + d^2) \\ &+ h^2\sin^2\zeta\cos^2(\psi-\eta)\sin^2\theta \\ &- 2dh\sin\zeta\sin\theta\sin(\psi-\eta) \\ &+ h^2\sin\zeta\cos\zeta\sin(2\theta)\cos(\psi-\eta). \end{aligned} \quad (11)$$

Since the model of Eq. (10) is isotropic in the basal xy-plane, only the component of the magnetic field along the z axis, $h_z = h\cos\zeta$, and its projection on the basal plane, $h_\perp = \sqrt{h_x^2 + h_y^2} = h\sin\zeta$, are of importance in determining the equilibrium distributions $\theta(x,y)$ and $\psi(x,y)$. By rescaling spatial variables and the energy, the number of control parameters is reduced:

$$\begin{aligned} x_0 &= \sqrt{\frac{A\lambda}{|K|}}, \qquad & h_0 &= \sqrt{|K|}, \\ D_0 &= \frac{4}{\pi}\sqrt{\frac{A|K|}{\lambda}}, \qquad & K &= \lambda B - d^2. \end{aligned} \quad (12)$$

In the equations of (12), x_0 is the reduced length, h_0 is the reduced magnetic field — also known as the spin-flop field — and D_0 is the reduced strength of the inhomogeneous Dzyaloshinskii-Moriya interaction. At zero field, x_0 corresponds roughly to the size of an isolated domain wall between homogeneous states, and D_0 is equal to the lowest value of D that stabilizes modulated states. Furthermore, an effective anisotropy constant K is introduced as well, which acts on the staggered magnetization. In this sense, K can be interpreted as an analogue to a constant of uniaxial anisotropy in ferromagnets.

The total magnetization, induced by $\mathbf{d}$, in the basal xy-plane orientates itself in a way that causes the staggered magnetization to rotate into the plane perpendicular to the direction of $h_\perp$, an effect which becomes stronger with equally stronger d and in-plane components of $\mathbf{l}$. One may now define the deviation of the staggered magnetization from the aforementioned plane as $\epsilon = |\psi - \eta - \pi/2|$, and assume it is small. Minimizing Eq. (10) with respect to ϵ yields:

$$\epsilon = \left| \psi - \eta - \frac{\pi}{2} \right| = \left| \frac{h\cos\zeta\cos\theta}{d + h\sin\zeta\sin\theta} \right|. \quad (13)$$

For $d \gg h$, Eq. (13) supports the earlier assumption $\epsilon \ll 1$. We now further assume that $\epsilon = 0$, due to the staggered magnetization being always restricted to the plane perpendicular to $h_\perp$. This allows us to substitute $\psi - \eta = \pi/2$ in the energy density of Eq. (11), which can then be simplified using the scaled quantities of (12) and dropping terms independent of θ to obtain $\tilde{w} = |K|\Phi(\theta)/\lambda$, with

$$\begin{aligned} \Phi(\theta) &= \mathrm{sgn}(K)\left(1 - \frac{h^2}{K}\cos^2\zeta\right)(\sin\theta - \nu)^2; \\ \nu &= \frac{dh\sin\zeta}{K - h^2\cos^2\zeta} = \frac{dh_\perp}{K - h_z^2}. \end{aligned} \tag{14}$$

The results of Eqs. (10) and (14) will prove to be useful in investigating the main properties of structures in anti-ferromagnetic materials.

2.2 Application to homogeneous and spiral states

2.2.1 Homogeneous states

Homogeneous states of the anti-ferromagnetic material are described by Eq. (14), with two different types of orderings according to the sign of K.

Starting with $K > 0$, the so-called easy axis system, the anti-ferromagnetic phase with properties $\mathbf{h} \parallel z, \mathbf{m} = 0$ has the lowest energy in magnetic fields $h = h_z < h_0$ along the tetragonal z axis, and in generally also at zero field. For $h = h_z, h_\perp = 0$, $\theta = 0$ for the anti-ferromagnetic phase. A spin-flop transition occurs when $h = h_z = h_0 = \sqrt{K}$, named so because $\mathbf{l}$ 'flops down' onto the basal xy plane, and generates a spin-flop phase where $\theta = \pi/2$. This causes a slight magnetization $|\mathbf{m}| \ll 1$, and from Eq. (8) one obtains for $|\mathbf{m}| \ll 1$ the components of this slight magnetization, $m_z = h/\lambda$ and $\sqrt{m_x^2 + m_y^2} = |m_\perp| = d/\lambda$. This means that the total magnetization increases linearly with increasing field h for $h_0 < h < \lambda$. This continues until the field reaches $h = h_{\mathrm{ex}} = \lambda$ and a spin-flip transition occurs, in which the spin-flop phase transforms into the 'paramagnetic' phase with parameters $|\mathbf{m}| = 1$, $\mathbf{l} = 0$.

The staggered magnetization $\mathbf{l}$ rotates away from the tetragonal z axis towards the basal xy plane for an increasing magnetic field deviating from the tetragonal axis. This justifies to describe relation between the angle measured from $\mathbf{l}$ to the z axis, θ, and the magnetic field as $\sin\theta = \nu$, for $\nu < 1$. The resulting phase is named the canted phase. A phase transition occurs at the critical value $\nu = 1$ — corresponding to the critical line $h_c(h_\perp, h_z)$ — resulting in the weak ferromagnetic phase where $\mathbf{l}$, now perpendicular to the applied field, lies in the xy plane, *i.e.* $\sin\theta = 1$. The phase diagram for this transition is given by Fig. 4.

At zero field for the easy plane system $K < 0$, the system has $\mathbf{l}$ already lying in the xy-plane with $(|\mathbf{m}| = d/\lambda)\perp\mathbf{n}$, which is therefore a weak ferro-

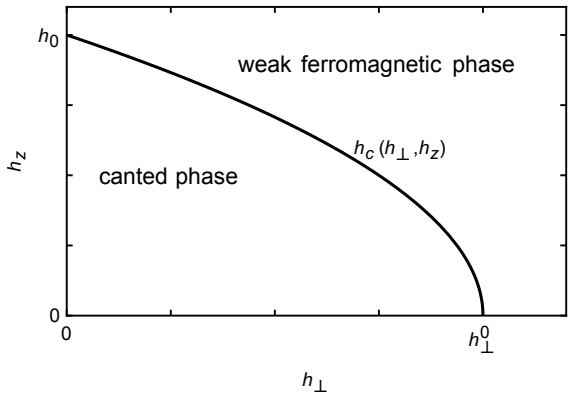

Figure 4: Phase diagram in $(h_\perp, h_z)$ space for homogeneous states in easy-axis system ($K > 0$). The critical line $h_c(h_\perp, h_z)$ is determined by the condition $\nu = 1$ in Eq. (13).

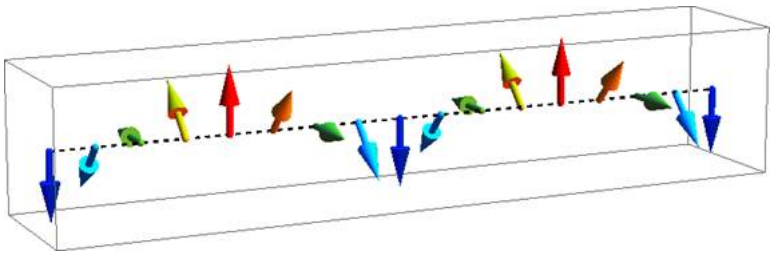

Figure 5: An example of a spiral state in anti-ferromagnetic materials. Figure reprinted from Everschor [11].

magnetic phase. At non-zero field, the system behaves similarly to the easy axis system for $h_z > h_0$.

2.2.2 Spiral states

Spiral structures, for example the structure represented in Fig. 5, are obtained by minimizing Eq. (10). This results, depending on the type of Lifshitz invariants w_D used, in helicoids for materials of crystallographic class D_{2d}, or in cycloids for materials of class C_{nv}. These two modulated structures differ in the way the staggered magnetization $\mathbf{l}$ rotates, which yields $\psi = \pi/2$ for helicoids and $\psi = 0$ for cycloids, *i.e.*, the propagation direction for helicoids and cycloids are perpendicular to each other. The Lifshitz invariants w_D are then:

$$\begin{aligned} w_D &= D\frac{\partial\theta}{\partial x}, \text{ for helicoids;} \\ w_D &= D\frac{\partial\theta}{\partial y}, \text{ for cycloids.} \end{aligned} \tag{15}$$

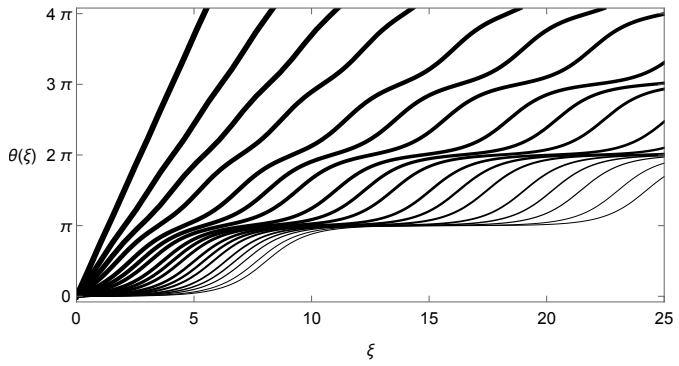

Figure 6: Solutions of Eq. (17) $\theta(\xi, E)$ corresponding to multiple values of $E > 0$. Thinner lines correspond to lower values of E.

The energy of Eq. (10) becomes a two-dimensional problem, which we simplify by noting from Eq. (15) one can obtain a reduced length $\xi = x_i/x_0$ from the reduced unit x_0 of Eq. (12). Applying this in Eq. (10), and absorbing the ξ-perpendicular integrations in the z direction yields:

$$\tilde{\tilde{W}} = \sqrt{\frac{A|K|}{\lambda}} \int \mathrm{d}\xi \, \left\{ \left(\frac{\partial \theta}{\partial \xi} \right)^2 + \Phi(\theta) + \frac{4D}{\pi D_0} \left(\frac{\partial \theta}{\partial \xi} \right) \right\}. \tag{16}$$

Applying the Euler equation on Eq. (16) then yields:

$$\left(\frac{\partial \theta}{\partial \xi} \right)^2 - \Phi(\theta) = E, \tag{17}$$

where E is an integration constant. The behaviour of the system depends on the three possible values of E: $E < 0$ or closed trajectories, $E = 0$, and $E > 0$ or open trajectories. Since $E < 0$ describes states which do not minimize inhomogeneous Dzyaloshinskii-Moriya interactions, open trajectories $E > 0$ will be discussed solely from this point. Integrating Eq. (17) with $\Phi(\theta)$ from Eq. (14) yields a set of solutions $\theta(\xi, E)$. These solutions are parametrized by the integration constant E, and numerical integrations of Eq. (14) with varying values of $E > 0$ are shown in Fig. 6.

Averaging the energy from Eq. (16), by dividing over a period Ξ, yields an averaged energy $\bar{w}$. This averaged energy can, by using Eq. (17), be

written as functions of the integration constant E[1]:

$$\bar{w} = \sqrt{\frac{A|K|}{\lambda}} \frac{1}{\Xi(E)} \int_0^{2\pi} \frac{E + 2\Phi(\theta)}{\sqrt{\Phi(\theta) + E}} \, \mathrm{d}\theta + \frac{2\pi D}{\Xi(E)}; \tag{18}$$

$$\Xi(E) = \int_0^{2\pi} \frac{\mathrm{d}\theta}{\sqrt{\Phi(\theta) + E}}. \tag{19}$$

Despite Eq. (17) being independent from inhomogeneous chiral Dzyaloshinskii-Moriya interactions, the averaged energy $\bar{w}$ from Eq. (18) does, however, depend on Lifshitz invariants contributions. Since the values $\bar{w}$ vary with different solutions of $\theta(\xi, E)$, this implies the equation $\mathrm{d}\bar{w}/\mathrm{d}E = 0$, used to determine the optimal values $\tilde{E}$, can be rewritten as:

$$\int_0^{2\pi} \mathrm{d}\theta \, \sqrt{\Phi(\theta) + E} = \frac{4D}{D_0}. \tag{20}$$

2.2.3 Calculating energies of homogeneous and spiral states

In homogeneous states, as noted before in Subsubsection 2.2.1, only the term $\tilde{w} = |K|\Phi(\theta)/\lambda$ is used for calculating the energy $\tilde{W}$. There are several types of homogeneous states, and we shall, for indicative purposes, discuss two of them: the anti-ferromagnetic phase and the spin-flop phase.

For the anti-ferromagnetic phase, $\theta = 0$, and therefore the *average* energy of the *system* is zero. More interesting is the spin-flop phase, with $\theta = \frac{\pi}{2}$, which simplifies the energy integral over $\tilde{w}$ drastically. For a system described by polar coordinates, the energy density ϵ_{SF} is given by:

$$\begin{aligned}
\epsilon_{\mathrm{SF}} &= \frac{1}{\pi R^2} \int_0^R \mathrm{d}\rho \, \tilde{w}(\theta = \frac{\pi}{2})\rho \\
&= \frac{1}{\pi R^2} \int_0^R \mathrm{d}\rho \, \frac{|K|}{\lambda} \mathrm{sgn}(K) \left(1 - \frac{h_z^2}{h_0^2}\right) (1-\nu)^2 \rho \\
&= \frac{K(1-\nu)^2}{\pi R^2 \lambda} \left(1 - \frac{h_z^2}{h_0^2}\right) \int_0^R \mathrm{d}\rho \, \rho \\
&= \frac{K(1-\nu)^2}{2\pi\lambda} \left(1 - \frac{h_z^2}{h_0^2}\right).
\end{aligned} \tag{21}$$

The energy density of the spin-flop phase is therefore independent of the Dzyaloshinskii-Moriya constant D.

For spiral states, one can calculate the average energy by evaluating the integral of Eq. (16). This, however, must be preceded by finding the value of the integration constant E and the correct form of the function $\theta(\xi)$, for

[1] The original article of Bogdanov *et al.* (2002) [10] contains two typos in the equation for $\bar{w}$.

a value of the Dzyaloshinskii-Moriya constant D and external magnetic field h.

Firstly, we evaluate the integral of Eq. (20) for a certain value of h, since from Eq. (14) we know $\Phi(\theta)$ depends on h, for various values of E, until a certain value of E is reached such that the integral yields a value $4D/D_0$ for a desired value of D. Secondly, this found value of E is then used to solve Eq. (17), in order to obtain an appropriate (elliptic) function $\theta(\xi, E)$. Thirdly, using $\Xi(E)$ from Eq. (18) as its upper boundary and zero as its lower boundary, the integral of Eq. (16) can then be evaluated for the desired values of h and D.

For comparison with other modulated structures, one can use the density of the spiral state energy, which is the energy divided by the length of the state:

$$\epsilon_{\text{spi}} = \frac{\tilde{\tilde{W}}}{\Xi(E)}. \tag{22}$$

2.2.4 Phase diagram for homogeneous and spiral states

Now that methods of calculating energy densities of homogeneous and spiral states are known, a phase diagram of anti-ferromagnetic materials can be constructed. Again, we take favourable circumstances, the most notable being the external magnetic field to be completely aligned along the tetragonal axis of the material, i.e., $h = h_z$. Consequently, this yields $h_\perp = 0, \nu = 0$ and simplifies the spin-flop energy density ϵ_{SF} from Eq. (21).

The phase boundaries are then mainly determined by the *critical* values D_c of the Dzyaloshinskii-Moriya interaction constant. These are defined[2] as:

$$\frac{D_c}{D_0} = \sqrt{\left|\frac{h^2}{K} - 1\right|}, \tag{23}$$

for easy-plane systems ($K < 0$) and easy-axis systems ($K > 0$) for an external magnetic field larger than the spin-flop field ($h > h_0$). For easy-axis systems where $h < h_0$, the critical values D_c are given by:

$$\frac{D_c}{D_0} = \sqrt{1 - \frac{h^2}{h^0}}. \tag{24}$$

Furthermore, let us introduce two new quantities to measure the *relative* external magnetic field and Dzyaloshinskii-Moriya interaction constant respectively:

$$\bar{h} = \frac{h}{h_0}; \qquad \bar{D} = \frac{D}{D_0}, \bar{D}_c = \frac{D_c}{D_0}. \tag{25}$$

[2]For more details on the derivation of Eqs. (23) and (24) , see Bogdanov *et al.* (2002) [10].

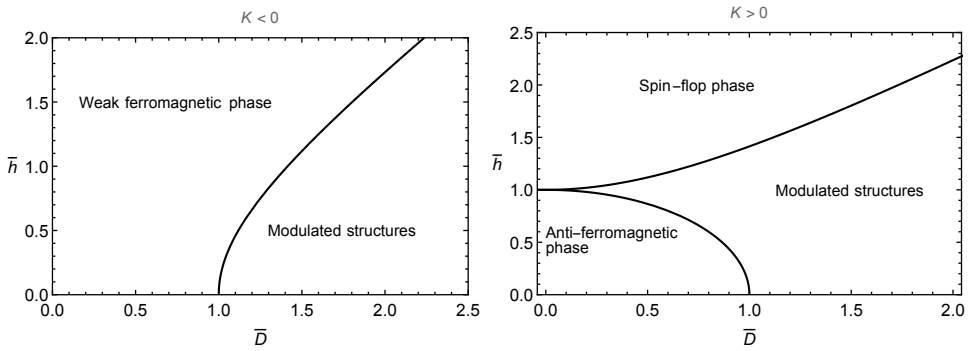

(a) Easy-plane system. (b) Easy-axis system.

Figure 7: Phase diagrams for anti-ferromagnetic material lacking inversion symmetry, in an external magnetic field along the tetragonal axis of the material.

Eqs. (23) and (24) can then be rewritten as

$$\bar{D}_c = \sqrt{\left|\mathrm{sgn}(K)\bar{h}^2 - 1\right|}; \qquad \bar{D}_c = \sqrt{1 - \bar{h}^2}, \tag{26}$$

respectively.

Using Eq. (26), one can construct phase diagrams for easy-axis and easy-plane systems. The constructed diagrams, plotted in the $(\bar{D}, \bar{h})$ parameter space, are given in Fig. 7.

3 The skyrmion configuration

In Section 2, we set up a model for magnetic structures, and their energies, in anti-ferromagnetic materials. Now, we shift our attention to the skyrmion configuration in order to calculate its energy in various circumstances, and compare this energy with those of the homogeneous and spiral states.

3.1 Model of the skyrmion configuration

As we have seen in Subsection 1.1, skyrmion configurations — like other rotationally invariant systems — are spatially described by cylindrical coordinates. In our case, we define the spatial variables $\mathbf{x}$ of Eq. (10) as

$$\mathbf{x} = x_0(\rho\cos\phi, \rho\sin\phi, z), \tag{27}$$

where x_0 is the reduced length introduced in Eq. (12). Since our system is rotationally invariant, the Lifshitz invariants w_D, which normally depend on the type of material used, can be written, for all types of materials, as:

$$w_D = D\left[\cos\phi\frac{\partial\theta}{\partial x} + \sin\phi\frac{\partial\theta}{\partial y} - \sin\theta\cos\theta\left(\sin\phi\frac{\partial\phi}{\partial x} - \cos\phi\frac{\partial\phi}{\partial y}\right)\right]. \tag{28}$$

The rotational invariance of the skyrmion also means it prefers to align its rotational axis along the tetragonal axis of the material. It is therefore convenient to choose the external magnetic field h to be aligned along the tetragonal z axis, i.e., $h = h_z$. This leads directly to $h_\perp = 0$, and using Eq. (14) then yields:

$$\tilde{w} = \frac{|K|}{\lambda}\mathrm{sgn}(K)\left(1 - \frac{h^2}{K}\right)\sin^2\theta. \tag{29}$$

Using Eq. (27), (28), (29), the reduced quantities used in Eq. (12), (25), and the jacobian determinant for cylindrical coordinates into the energy of Eq. (10), one obtains the energy of a skyrmion of size R:

$$\begin{aligned}\tilde{W}_{\mathrm{sk}}(R) = \frac{|K|}{\lambda}\int_0^R \mathrm{d}\rho\Bigg\{&\left(\frac{\mathrm{d}\theta}{\mathrm{d}\rho}\right)^2 + \frac{\sin^2\theta}{\rho^2} + \frac{8}{\pi}\bar{D}\left(\frac{\mathrm{d}\theta}{\mathrm{d}\rho} + \frac{\sin\theta\cos\theta}{\rho}\right) + \\ &+ \mathrm{sgn}(K)(1-\bar{h}^2)\sin^2\theta\Bigg\}\rho.\end{aligned} \tag{30}$$

Using the Euler-Lagrange equations on Eq. (30) yields the equation of motion for $\theta(\rho)$:

$$\frac{\mathrm{d}^2\theta}{\mathrm{d}\rho^2} + \frac{1}{\rho}\frac{\mathrm{d}\theta}{\mathrm{d}\rho} - \frac{\sin\theta\cos\theta}{\rho^2} + \frac{8}{\pi}\bar{D}\frac{\sin^2\theta}{\rho} - \left(1-\bar{h}\right)\sin\theta\cos\theta = 0, \tag{31}$$

with boundary conditions $\theta(0) = \pi$ and $\theta(R) = 0$ for *localized* structures in $h < h_0$, and $\theta(0) = \pi, \theta(R) = \pi/2$ for *delocalized* structures in $h > h_0$. From this point, we will discuss the localized structures in $h < h_0$.

3.2 Calculating energies of skyrmion configurations

As one can observe from Eq. (30), the energy of a skyrmion configuration of size R is determined by the parameters $\bar{h}$ and $\bar{D}$, and an appropriate function $\theta(\rho)$ with boundary conditions $\theta(0) = \pi, \theta(R) = 0$. In fact, the position of the skyrmion configuration in the $(\bar{D}, \bar{h})$ parameter space influences the function $\theta(\rho)$. We therefore investigate the stability of skyrmion configurations with respect to the states described in the phase diagrams of Fig. 7, since these diagrams are plotted in the $(\bar{D}, \bar{h})$ parameter space, for the tetragonally aligned external magnetic field $h = h_z$ the skyrmion configuration model of Subsection 3.1 is based on.

To investigate a skyrmion configuration, we choose a single point in the $(\bar{D}, \bar{h})$ parameter space, and — for convenience — let us assume an easy-axis system, i.e. $K > 0$, so that we can use the phase diagram of Fig. 7b to compare with other states in the anti-ferromagnetic material. We then define an *energy density* $\epsilon_{\mathrm{sk}}(R)$ of the skyrmion configuration of size R:

$$\epsilon_{\mathrm{sk}}(R) = \frac{1}{\pi R^2} \tilde{W}_{\mathrm{sk}}(R). \tag{32}$$

The energy density ϵ_{sk} is calculated for various values of R, until the minimum value $\epsilon_{\mathrm{min}}(R_{\mathrm{min}})$ is found. We now know the minimal skyrmion energy density for one point in the $(\bar{D}, \bar{h})$ parameter space. Since we discuss the localized structures of $h < h_0$, i.e. $\bar{h} < 1$, the freedom in parameter $\bar{h}$ is restricted, and thus we choose two values of $\bar{h}$: $\bar{h} = \frac{1}{2}$, and $\bar{h} = \frac{1}{20}$. These choices reflect a noticeable external field, and a small external field, respectively.

We can now effectively calculate the minimum energy density ϵ_{min}, and its associated size R_{min}, at multiple points in the $(\bar{D}, \bar{h})$ space by varying $\bar{D}$, while using the previously chosen values of $\bar{h}$. The results shown in Fig. 8 show the results for both $\bar{h} = \frac{1}{2}$ and $\bar{h} = \frac{1}{20}$. One may notice from Fig. 8, that the choice of $\bar{h}$ is less important when investigating the behaviour of the skyrmion configuration, than the choice of $\bar{D}$.

When compared to the homogeneous anti-ferromagnetic phase described in Subsubsection 2.2.1, the skyrmion configuration is stable, i.e., it possesses a negative minimum energy density, for 5 out of 9 cases, where the values of $\bar{D}$ and $\bar{h}$ of the investigated skyrmion configuration were in the anti-ferromagnetic phase.

Calculated along with the skyrmion configuration up to $\bar{D} = 2$, the spiral state energy described in Subsubsection 2.2.2 — and its associated density ϵ_{spi} from Eq. (22) — was found to have a positive value for both $\bar{h} = \frac{1}{2}$ and $\bar{h} = \frac{1}{20}$. A comparison between the energy densities of the skyrmion and spiral states can be seen in Fig. 9. Since the skyrmion energy density tends to attain a negative value, this results in stable skyrmion configurations in the spiral states phase. Furthermore, Fig. 9 suggests the

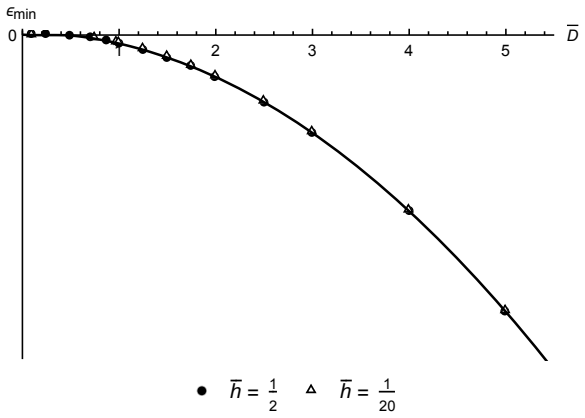

(a) $(\bar{D}, \epsilon_{min})$ plot.

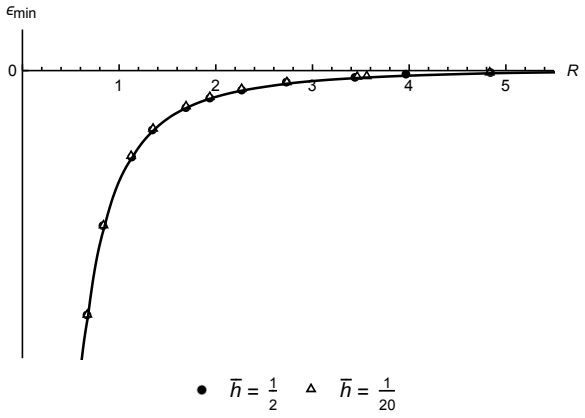

(b) $(R, \epsilon_{\min})$ plot.

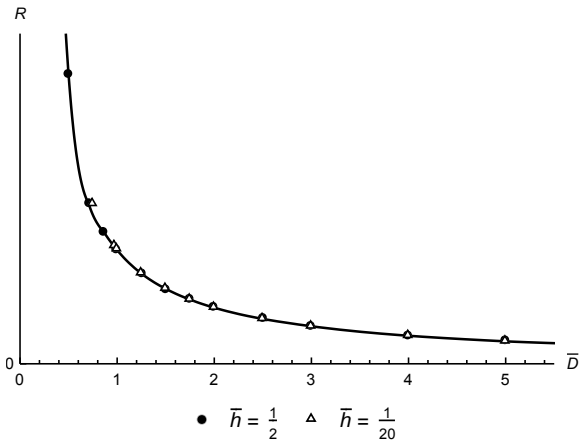

(c) $(\bar{D}, R)$ plot.

Figure 8: Obtained datasets for cases $\bar{h} = \frac{1}{2}, \bar{h} = \frac{1}{20}$. Notice the barely noticeable differences between the datasets for $\bar{h} = \frac{1}{2}$ and for $\bar{h} = \frac{1}{20}$.

skyrmion configuration is the most stable state found among the modulated structures phase, in the phase diagram of Fig. 7b, for $\bar{h} \leq \frac{1}{2}$ and $\bar{D} \geq \bar{D}_c$.

This yields a 'rough' area in the $(\bar{D}, \bar{h})$ parameter space, where one could find stable skyrmion configurations; this area is part of a skyrmion phase in $(\bar{D}, \bar{h})$ space, which is now partially identified, as can be seen in Fig. 10.

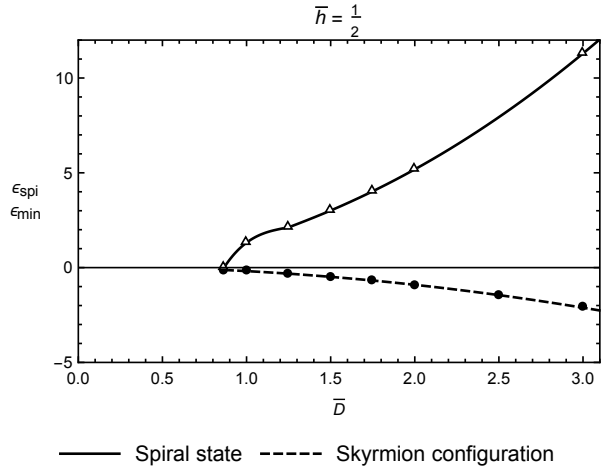

(a) Energy densities for $\bar{h} = \frac{1}{2}$.

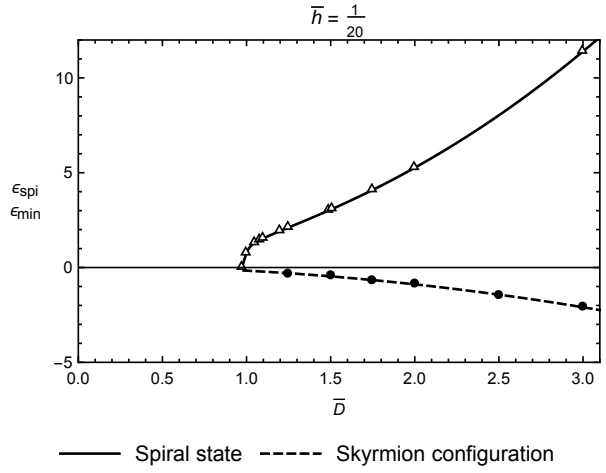

(b) Energy densities for $\bar{h} = \frac{1}{20}$.

Figure 9: Energy density plots of spiral and skyrmion states, plotted for the relevant area $\bar{D} \geq \bar{D}_c$.

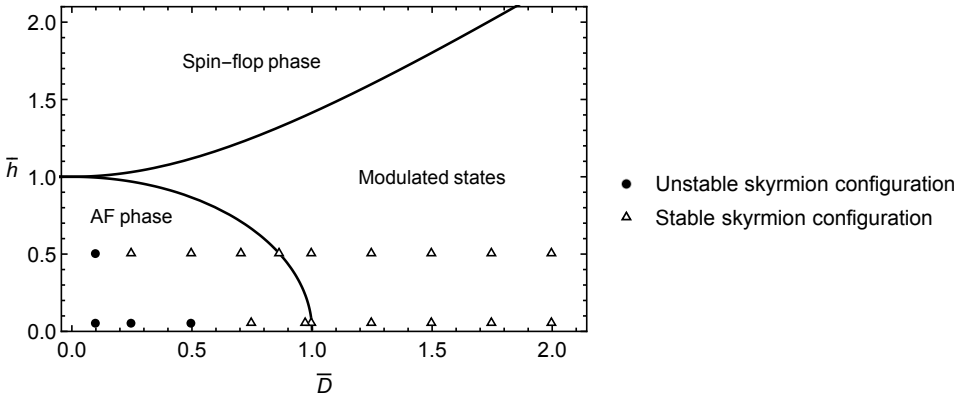

Figure 10: Stability, with respect to the homogeneous state of the anti-ferromagnetic (AF) phase and the spiral state, of various skyrmion configuration in the $(\bar{D}, \bar{h})$ parameter space.

4 Conclusions

In this Thesis, we found stable skyrmion configurations in anti-ferromagnetic materials with inversion asymmetry. Whether these skyrmion configurations are stable or not, depends on the strength D of the Dzyaloshinskii-Moriya interaction, and somewhat less on the strength h of the external field. For $\bar{h} = \frac{h}{h_0} \leq \frac{1}{2}$, with h_0 the so-called spin-flop field, the skyrmion configuration as a stable state is dominant, especially among other modulated structures governed by D.

For future investigations, a further refinement of the 'primitive' phase diagram of Fig. 10 is a prime priority. This can be achieved by investigating more coordinates of $(\bar{D}, \bar{h})$ for the skyrmion configuration. Since stable skyrmion configurations tend to occur near the critical line $\bar{D}_c = D_c/D_0$ between anti-ferromagnetic and modulated chiral phases, it is recommendable that future Monte-Carlo simulations on the skyrmion phase should begin near this critical line. Another guide for future research is to use the model and methods described in this Thesis for delocalized structures, where $h > h_0$.

References

[1] M.P. Marder, *Condensed Matter Physics*, second edition, Chapter 24, John Wiley & Sons (2010).

[2] I.E. Dzyaloshinskii[3], Sov. Phys. JETP **5**, 1259–1272 (1957)

[3] T. Moriya, Phys. Rev. Lett. **4**, 228–230 (1960).

[4] T.H.R. Skyrme, Nucl. Phys. **32**, 556–569 (1962).

[5] A. Mühlbauer *et al.*, Phys. Rev. Lett. **102**, 186602 (2009).

[6] S. Heinze *et al.*, Nature Physics **7**, 713–718 (2011).

[7] A. Fert, V. Cros, J. Sampaio, Nature Nanotechnology **8**, 152–156 (2013).

[8] S.J. Venema, *Magnetic phase diagrams of spin systems with inversion asymmetry*, Bachelor Thesis, Utrecht University (2014).

[9] M.E. Knoester, *Skyrmions driven by the spin Hall effect*, Bachelor Thesis, Utrecht University (2013).

[10] A.N. Bogdanov, U.K. Rößler, M. Wolf, K.-H. Müller, Phys. Rev. B **66**, 214410 (2002).

[11] K. Everschor, *Current-Induced Dynamics of Chiral Magnetic Structures; Skyrmions, Emergent Electrodynamics and Spin-Transfer Torques*, Doctoral Thesis, University of Cologne (2012).

[3] Transliterated as 'Dzialoshinskii' in the original translated article, other common transliterations are 'Dzyaloshinsky', 'Dzyaloshinskiy', *etc.*